This document is the Accepted Manuscript version of a Published Work that appeared in final form in J. Mater. Chem. A, 2015, 3, 4892–4902 DOI: 10.1039/C4TA05807K

Solution processed organic solar cells based on A–D–D′–D–A small molecule with benzo[1,2-*b*:4,5-*b*′]dithiophene donor (D′) unit, cyclopentadithiophene donor (D) and ethylrhodanine acceptor unit having 6% light to energy conversion efficiency

Challuri Vijay Kumar; Lydia Cabau; Emmanuel N. Koukaras; Aurelien Viterisi: Ganesh D. Sharma; Emilio Palomares

[a]*Institute of Chemical Research of Catalonia (ICIQ), Avda. Països Catalans 16, E-43007 Tarragona, Spain. E-mail: epalomares@iciq.es*
[b]*Institute of Chemical Engineering Sciences, Foundation for Research & Technology, Hellas, Stadiou Str. Platani, Patras, 26504, Greece*
[c]*Molecular Engineering Laboratory, Department of Physics, University of Patras, Patras, 26500, Greece*
[d]*R&D Center for Engineering and Science, JEC Group of Colleges, Jaipur Engineering College, Kukas, Jaipur 303101, India. E-mail: gdsharma273@gmail.com;sharmagd_in@yahoo.com*
[e]*Catalan Institution for Research and Advance Studies (ICREA), Avda. Lluis Companys 23, E-08010 Barcelona, Spain*

Solution processed small molecule A–D–D′–D–A, denoted as **BDT(CDTRH)$_2$**, consists of 2-ethylhexoxy substituted **BDT** (donor D' unit) as the central building block and 3-ethylrhodanine (RH) as the end capped terminal (acceptor group) unit, with a π-linkage of cyclopentadithiophene (CDT) (donor D). We have designed and synthesized it, and we have investigated its optical and electrochemical properties, finding that its energy levels are compatible with the energy levels of fullerene derivatives for efficient exciton dissociation. This small molecule has been used as an electron donor along with $PC_{71}BM$ as the electron acceptor for the fabrication of solution processed small molecule bulk heterojunction (BHJ)

solar cells. The BHJ solar cell processed with **BDT(CDTRH)$_2$** : $PC_{71}BM$ (1 : 1 wt ratio) showed a power conversion efficiency (PCE) of 4.58% with J_{sc} = 8.66 mA cm^{-2}, V_{oc} = 0.98 V and FF = 0.54. The high V_{oc} value of the device has been attributed to the deeper HOMO energy level of **BDT(CDTRH)$_2$**. The overall PCE of the device has been increased up to 6.02% (J_{sc} = 10.42 mA cm^{-2}, V_{oc} = 0.94 V FF = 0.62) when the blend was processed with 3% v/v CN/CF solvent. This increase is mainly due to an increase in J_{sc} and FF, which was linked to the increase in crystallinity and favorable nanomorphology of the active layer improving exciton dissociation and achieving a more balanced charge transport in the device.

Introduction

Organic solar cells based on solution processed active layers consisting of small molecule (SM):fullerene blends have attracted a lot of attention on account of their advantages, such as having a large area, being flexible, producing light weight devices by roll to roll printing techniques, as well as their high purity and discrete molecular weight.[1] They can be a viable alternative to the polymer:fullerene systems, as demonstrated by the impressive power conversion efficiencies, in the range of 8–10%.[2] At present, the research on solution processed small molecule (SM)-based organics solar cells is targeted to achieve higher PCEs by designing and synthesizing new organic small molecules with D–A–D or A–D–A structures.[3] The most promising organic small molecule donor materials for photovoltaic applications are generally built by connecting various electron donating (donor) and electron accepting (acceptor) units through a π-conjugated spacer.[4] Among the different donor units used in the D–A copolymers, benzo[1,2-*b*:4,5-*b*′]dithiophene (**BDT**) is one of the most promising electron-donor units for applications in high-performance polymer semiconductors. Its large planar π-conjugated structure promotes enhanced π–π stacking and improves hole mobility.[5] Compared to one dimensional (1D) **BDT** based conjugated polymers, the two dimensional (2D) **BDT** polymers based solar cells show high V_{oc} due to its deeper HOMO energy levels. Recently, a D–A copolymer with benzodithiophene (D) unit showed a PCE of 8.3% when processed with 1-chloronaphthalene (CN) as an additive.[6] The efficient photovoltaic response of these 2D **BDT**copolymers makes them a promising donor material for solution processed small molecule organic solar cells (SMOSCs).[7] Therefore, small molecules with high efficiency could be designed by tailoring the HOMO and LUMO energy levels of the 2D **BDT** unit by introducing appropriate electron accepting units and π-bridge linkers.

A series of dye building blocks, including 3-ethylrhodanine (RH), 1,3-indandione and 1,3-dimethylbarbituric acid, have been introduced as electron accepting units along with electron rich oligothiophenes and/or **BDT** providing low bandgap small molecule donor materials.[8] A PCE up to 8.12% has been achieved with a small molecule using thienyl benzodithiophene (**BDT**) as core and 3-ethylrhodanine as terminal group.[8b] Bazan *et al.* reported $DTS(PTTh_2)_2$ (ref. 9) and $DTS(FBTTh_2)_2$ (ref. 10) using dithienosilole (DTS) as a donor core with[1,2,5]-thiadiazolo-[3,4-*c*]-pyridine or fluorobenzothiadiazole as pendant moieties, both of which displayed promising photovoltaic performance with a PCE of up to 9.02%.[10b] Both Li *et al.* and Chen *et*

al. synthesized two 2D small molecules, D2 and DR3TBDTT with an appropriate A–π–D–π–A molecular structure, which showed excellent photovoltaic performance with PCE, up to 6.75% and 8.12%, respectively.[11,12]

Many promising end group acceptors, *i.e.* dicyanovinyl,[13,14] alkyl cyanoacetate[15–18] and 3-ethylrhodanine[19,20] have been used for conjugated small molecules with A–D–A structure. Chen*et al.* reported an A–D–A small molecule comprised of a 3-ethylrhodamine end group, yielding a certified PCE of 7.6%.[21] More recently, using a 2D conjugated small molecule (SMPV1), the best PCE of OSCs reached 8% and 10% for a single junction and a double tandem OSCs,[22] indicating a promising potential for BHJ organic solar cells based on these materials at low cost.

In this work, we have synthesized a novel A–D–D′–D–A small molecule denoted as **BDT(CDTRH)$_2$** by employing **BDT** as core donor (D′) unit and 3-ethylrhodanine (RH) as electron withdrawing end groups, linked through a cyclopentadithiophene (CDT) (D) π spacer, and we have investigated its photophysical and electrochemical properties. CDT has been used as donor units in CDT–benzothiazole oligomer small molecules and showed a PCE of 1.61% when blended with fullerene derivatives.[23] We have used this small molecule as electron donor along with $PC_{71}BM$ as electron acceptor for the fabrication of solution processed BHJ organic solar cells. The optimized device with a blend of **BDT(CDTRH)$_2$**:$PC_{71}BM$ (1 : 1) processed with chloroform (CF) achieved a PCE of 4.58% with J_{sc} = 8.66 mA cm^{-2}, V_{oc} = 0.98 V and FF = 0.54. The high value of V_{oc} has been attributed to the deeper HOMO level of**BDT(CDTRH)$_2$**. The PCE was further improved to 6.07% when small a amount of CN (3% v/v) was added to the blend solution. The enhancement of PCE upon using solvent additives may be attributed to an increase in the crystallinity of the active layer film, an enhancement in the absorption profile and favorable domain sizes of the donor and electron molecules, leading to an improved charge transport.

Experimental part

General

Unless otherwise stated, all reagents were purchased from commercial sources and used without further purification. Dry $CHCl_3$ and toluene were obtained by passing them through an activated alumina column on a PureSolv™ solvent purification system (Innovative Technologies, Inc., MA). Flash column chromatography was carried out using Silica gel 60, 40–63 μm (Panreac Química SLU) as the stationary phase. Size exclusion chromatography was carried out in a large elution column (1000 mm × 38 mm) with Biobead SX3 (Bio-Rad Laboratories, Inc.) as the stationary phase. The eluent was passed through the column under gravity.

Instruments

UV-visible absorption spectra were measured with a 1 cm path-length quartz cell using a Shimadzu model 1700 spectrophotometer. Steady state fluorescence spectra were recorded on a Spex model Fluoromax-3 spectrofluorometer using a 1 cm quartz cell. All ^{1}H and ^{13}C NMR spectra were recorded on a Brüker AV 300 and AV 400 instruments, respectively, at a constant temperature of 300 K, unless otherwise stated. Chemical shifts are reported in parts per million and referenced to residual solvent. Coupling constants (*J*) are reported in hertz (Hz). Standard abbreviations indicating multiplicity were used as follows: m = multiplet, quint. = quintet, q = quartet, t = triplet, d = doublet, s = singlet, br = broad. MALDI TOF mass spectra were recorded on a Water Quattro micro (Water Inc, USA) apparatus. Cyclic voltammetric experiments were carried out with a PC-controlled CH instruments model CHI620C electrochemical analyzer. The elemental analysis was carried out at the Unidade de Análise Elemental at the University of Santiago de Compostela (USC) using a FISONS model EA1108.

Synthesis and characterization

The relevant synthetic route is outlined in Scheme 1. 6-bromo-4,4-dihexyl-4*H*-cyclopenta [2,1-*b*:3,4-*b*′] dithiophene-2-carbaldehyde (**1**)[24] and 2,6-bis(trimethyltin)-4,8-bis(2-ethylhexoxy) benzo-[1,2-*b*:4,5-*b*′]dithiophene (**2**)[25] were prepared according to literature procedures. **BDT**–**CPDT**–CHO (**3**) was synthesized by Stille coupling between **1** and **2** in refluxing toluene under Argon in the presence of $Pd(PPh_3)_4$, as a catalyst for 48 hours. The target compound **BDT(CDTRH)$_2$** was obtained using Knoevenagel condensation with 3-ethylrhodanine. To obtain the best possible performance in OSC devices, **BDT(CDTRH)$_2$** was purified by consecutive flash chromatography, size exclusion chromatography and recrystallization methods. This combination of techniques was found effective in removing most impurities, however one by-product remained in the final product, as seen in the ^{1}H NMR spectrum of **BDT(CDTRH)$_2$**. The corresponding NMR peaks could not be assigned to an exact structure, however, they are likely to correspond to a benzodithiophene derivative originating from precursor **2**. It was estimated that the amount of by product in the final product was inferior to 5% by NMR. **BDT(CDTRH)$_2$** was found to be soluble, as other organic solvents.

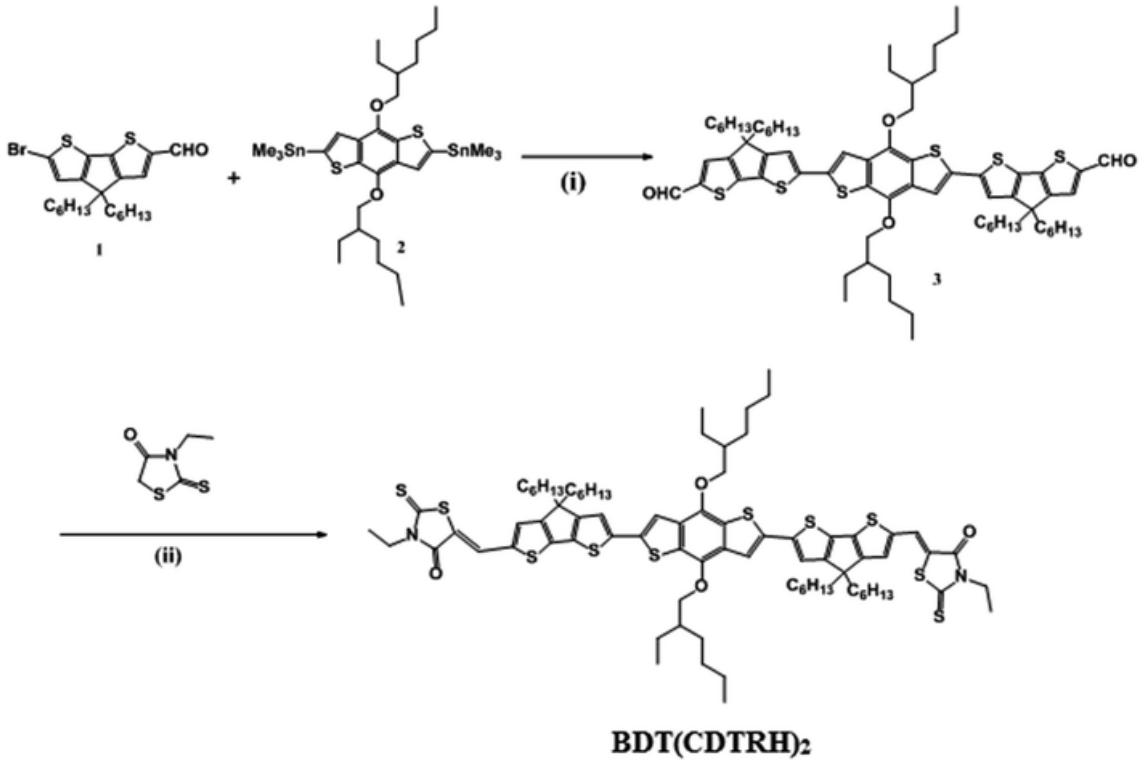

Scheme 1 Synthetic route of **BDT(CDTRH)$_2$**. (Reaction conditions): (i) $Pd(PPh_3)_4$, toluene, 48 h,

reflux (ii) dry $CHCl_3$, piperidine, 12 h, reflux.

Synthetic procedures

Synthesis of BDT–CPDT–CHO (3). A solution of 6-bromo-4,4-dihexyl-4*H*-cyclopenta[2,1-*b*:3,4-*b*′]dithiophene-2-carbaldehyde (**1**) (300 mg, 0.387 mmol) and 2,6-bis(trimethyltin)-4,8-bis(2-ethylhexoxy)benzo-[1,2-*b*:4,5-*b*′]dithiophene (**2**) (380 mg, 0.852 mmol) in dry toluene (20 mL) was degassed by performing two freeze/thaw cycles under Argon. $Pd(PPh_3)_4$ (44 mg, 0.04 mmol) was added to this solution. After being stirred for 48 h at 120 °C, the reaction mixture was poured into water and extracted with CH_2Cl_2. The organic layer was washed with water and then dried over $MgSO_4$. The solvent was removed under reduced pressure and the crude product was purified by column chromatography on silica gel using a mixture of CH_2Cl_2 and hexane (1 : 1) as eluent to afford compound **BDT**–**CPDT**–CHO (**3**) (290 mg, 39%). ^{1}H-NMR (300 MHz, $CDCl_3$) (Fig. S1 and S2 of ESI†) δ_H: 9.86 (S, 2H), 7.59 (S, 2H), 7.56 (S, 2H), 7.19 (S, 2H), 4.23 (d, J = 5.4 Hz) 1.92 (m, 2H), 1.69 (m, 8H), 1.46 (m, 4H), 1.26 (m, 44H), 0.81–0.90 (m, 24H). ^{13}CNMR (100 MHz, $CDCl_3$) δ: 182.23; 162.73; 157.92; 149.69; 147.37; 146.81; 143.87; 143.64; 141.64; 136.53; 135.46 133.58; 132.26; 129.78; 128.85; 119.29; 115.92; 54.05; 40.47; 38.49; 33.75; 31.34; 30.24; 29.47; 29.39; 29.02; 28.06; 24.39; 24.23; 23.53; 22.96; 22.72; 22.37; 14.00; 11.15. MALDI: *m*/*z* calcd for $C_{70}H_{94}O_4S_6$ 1190.55, found 1190.7 (Fig. S3 of ESI†).

Synthesis of BDT(CDTRH)$_2$. **BDT**–**CPDT**–CHO (**3**) (200 mg, 0.167 mmol) was dissolved in a solution of dry $CHCl_3$ (40 mL), a few drops of piperidine and then 3-ethylrhodanine (268 mg, 1.67 mmol) were added, and the resulting solution was refluxed and stirred for 24 h under argon. The reaction mixture was then extracted with CH_2Cl_2, washed with water, and dried over $MgSO_4$. The solvent was removed under reduced pressure and the crude product was purified by column chromatography on silica gel using CH_2Cl_2 and hexane (1 : 1) as eluent, followed by a subsequent size exclusion chromatography using THF as eluent. The solid was further purified by two consecutive recrystallizations carried out as follows: the solid was dissolved in 15 mL of $CHCl_3$, and poured by syringe through a 0.2 μm PTFE filter in a 250 mL graduated cylinder. A buffer layer (10 mL) consisting of a 1 : 1 mixture of $CHCl_3$: hexane was carefully poured over the solution (filtered through 0.2 μm PTFE filter). Finally, pure hexane was carefully poured over the buffer layer (filtered through 0.2 μm PTFE filter) up to the top of the graduated cylinder and the solution was left in the dark undisturbed. **BDT(CDTRH)$_2$** precipitated as dark blue shiny crystals over a period of approximately 2 to 3 weeks, after which period they were recovered by filtration and

washed with plenty of hexane (200 mL) (120 mg, 60%). ^{1}H-NMR (300 MHz, $CDCl_3$) (Fig. S4 and S5 of ESI†) δ_H: 7.84 (S, 2H), 7.45 (S, 2H), 7.21 (S, 2H), 7.14 (S, 2H), 4.19 (m, 8H), 1.90 (m, 2H), 1.61 (m, 8H), 1.43 (m, 4H), 1.16 (m, 50H), 0.80–0.91 (m, 24H), ^{13}C-NMR (100 MHz, $CDCl_3$) δ: 191.60; 167.22; 161.87; 159.50; 145.94; 143.95; 141.95; 139.06; 136.74; 136.015; 132.47; 128.90; 128; 126.22; 119.43; 115.89; 113.45; 54.36; 40.74; 39.96; 37.80; 31.60; 30.52; 29.62; 29.29; 24.70; 23.92; 23.21; 22.61; 14.25; 14.00; 12.28; 11.43. MALDI (Fig. S6 of ESI†): *m*/*z* calcd for $C_{80}H_{104}N_2O_4S_{10}$ 1476.52, found 1476.5196. Anal. calcd for $C_{80}H_{104}N_2O_4S_{10}$: C, 65.00; H, 7.09; N, 1.89; O, 4.33; S, 21.69. Found: C, 64.47; H, 7.36; N, 1.87; O, 4.66; S, 21.63.

Device fabrication and characterization

The BHJ organic solar cells were fabricated using the glass/ITO/PEDOT:PSS/**BDT(CDTRH)$_2$**:$PC_{71}BM$/Al device structure. The ITO coated glass substrates were ultrasonically cleaned consecutively in aqueous detergent, de-ionized water, isopropyl alcohol and acetone and finally dried under ambient conditions. An aqueous solution of PEDOT:PSS (Heraeus, Clevios P VP, Al 4083) was spin cast on the ITO substrates to obtain a film having a thickness of about 40 nm. The PEDOT:PSS film was then dried for 10 min at a temperature of 120 °C in ambient conditions. Mixtures of **BDT(CDTRH)$_2$** with $PC_{71}BM$ with weight ratios of 1 : 0.5, 1 : 1, and 1 : 2 and 1 : 2.5 in chloroform (CF) were prepared and then spin-cast onto the PEDOT:PSS layer and dried overnight at ambient atmosphere. The devices were further fabricated by the use of 1%, 2%, 3% and 4%CN processing additive during the spin casting step (spinning speed was about 2000 rpm). The concentration of the **BDT(CDTRH)$_2$**:$PC_{71}BM$ blend was 20 mg mL^{-1}. The thickness of the active layer was in between 85–90 nm. Finally, the aluminium (Al) top electrode was thermally deposited on the active layer at a vacuum of 10^{-5} Torr through a shadow mask of area of 0.20 cm^2. All devices were fabricated and tested in ambient atmosphere without encapsulation. The hole-only and electron-only devices with ITO/PEODT:PSS/**BDT(CDTRH)$_2$**:$PC_{71}BM$/Au and ITO/Al/**BDT(CDTRH)$_2$**:$PC_{71}BM$/Al architectures were also fabricated in an analogous way, in order to measure the hole and electron mobility, respectively.

The current–voltage characteristics of the BHJ organic solar cells were measured using a computer controlled Keithley 238 source meter under simulated AM1.5G illumination of 100 mW cm^{-2}. A Xenon light source coupled with optical filter was used to give the stimulated irradiance at the surface of the devices. The incident photon to current efficiency (IPCE) of the devices was measured illuminating the device through the light source and monochromator and the resulting current was measured using a Keithley electrometer under short circuit conditions.

Results and discussion

Photophysical and electrochemical properties

Fig. 1 shows the UV-visible absorption spectra of **BDT(CDTRH)$_2$** in a chloroform solution and a thin film spin coated on a quartz substrate. In solution, **BDT(CDTRH)$_2$** exhibits an absorption peak around 582 nm with a molar extinction coefficient of 7.8×10^4 M^{-1} cm^{-1}. However, the **BDT(CDTRH)$_2$** film shows a broader absorption band, covering from 400 to 800 nm with an absorption peak around 618 nm and also exhibits a vibronic shoulder at 662 nm, indicating an effective π–π packing between the molecules' backbones in solid state.[26] The optical bandgap of **BDT(CDTRH)$_2$** was estimated from the onset absorption edge in its absorption spectra in thin film, and is about 1.72 eV. The low bandgap of **BDT(CDTRH)$_2$** is attributed to the ethylrhodanine acceptor moiety.[27] The absorption spectra of **BDT(CDTRH)$_2$** in thin films exhibits a broader absorption profile from 550 nm to 720 nm and a low bandgap, which increases light harvesting when used as donor in the active layer in organic solar cells. Cyclic voltammetry (CV) was used to estimate approximate HOMO and LUMO energy levels of **BDT(CDTRH)$_2$**. The HOMO and LUMO energy levels of the **BDT(CDTRH)$_2$**, calculated from the onset oxidation and reduction potential are −5.38 eV and −3.54 eV, respectively. The electrochemical bandgap of **BDT(CDTRH)$_2$** is 1.80 eV. The optical and electrochemical band gap of **BDT(CDTRH)$_2$** is similar to other small molecules reported in literature.[20]Considering that the $PC_{71}BM$ acceptor has HOMO and LUMO levels of −6.1 eV and −4.0 eV, respectively, the LUMO energy difference (>0.3 eV) between the donor and acceptor is large enough for the separation of excitons,[28] which is beneficial for increasing the short circuit current in **BDT(CDTRH)$_2$** based organic solar cells.

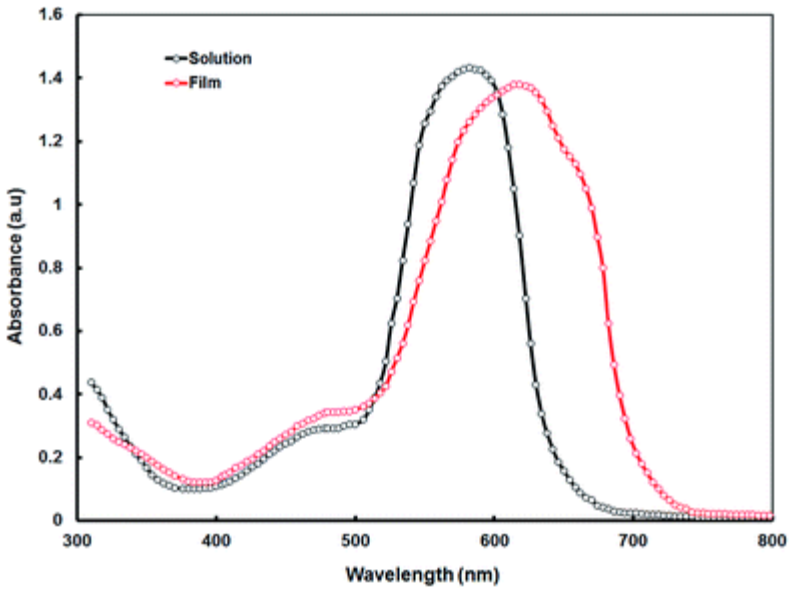

Fig. 1 Absorption spectra of **BDT(CDTRH)$_2$** in dilute solution of CF and thin film cast from CF.

Theoretical calculations

We have additionally performed a theoretical study on the **BDT(CDTRH)$_2$** molecular structure within the framework of density functional theory (DFT) and time-dependent density functional theory (TD-DFT). The initial geometry optimization calculations

were performed employing the gradient corrected functional PBE[29] of Perdew, Burke and Ernzerhof. The triple-ζquality TZVP basis set[30] was used for all of the calculations. At this stage of the calculations, to increase the computational efficiency (without loss in accuracy), the resolution of the identity method[31] was used for the treatment of the two-electron integrals. Subsequent geometry optimizations were further performed using the hybrid exchange–correlation functional B3LYP,[32] as well as Truhlar's meta-hybrid exchange–correlation functional M06 (ref. 33) and the same basis set. Tight convergence criteria were placed for the SCF energy (up to 10^{-7} Eh) and the one-electron density (rms of the density matrix up to 10^{-8}), as well as for the norm of the cartesian gradient (residual forces both average and maximum smaller than 1.5×10^{-5} a.u.) and residual displacements (both average and maximum smaller than 6×10^{-5} a.u.). Solvent effects were included for chloroform (CF) using the integral equation formalism variant of the Polarizable Continuum Model (IEFPCM), as implemented in the Gaussian package.[34] The first round of geometry optimization was performed using the Turbomole package.[35] All of the follow up calculations were performed using the Gaussian package.[34]

The TD-DFT excited state calculations were performed to calculate the optical gap of **BDT(CDTRH)$_2$** employing the same functionals and basis set on the corresponding ground state structures. The UV/vis spectra were calculated using the B3LYP and M06 (that provides leveled performance over transition type[36,37]) functionals.

For the geometry optimization of the **BDT(CDTRH)$_2$** molecular structure, several rotamers were examined as initial geometries, including aliphatic configurations (details are given in the ESI†). Vibrational analysis revealed that the final optimized structure is a true local (if not global) minimum and that none of the vibrational modes had imaginary eigen frequencies. The**BDT(CDTRH)$_2$** structure is for the most part planar, with a tilting of the outer groups relative to the central benzodithiophene group by dihedral angles in the range of 17°–27° (depending on the functional used and the presence of solvent). We have calculated the HOMO and LUMO energy levels and the optical gaps, defined here as energetically lowest, allowed vertical electronic excitation, employing the PBE, M06, and B3LYP functionals. In Table 1, in addition to the frontier orbitals' energy levels, we also provide the optical gap, the main contributions to the first excitation as well as the wavelength of the first excitation and of the excitations with the largest oscillator strengths. In Table 1, we also provide the character of the first allowed excitations only for contributions larger than 4%. The first excitation, as calculated by each of the functionals, clearly exhibits a strong single-configuration character, with only marginal (if any) to moderate secondary contributions.

Table 1 Calculated properties of **BDT(CDTRH)$_2$**. Specifically, HOMO and LUMO energies (eV), HOMO–LUMO gap (eV), HL, Optical gap (eV), OG with corresponding oscillator strengths, *f*, the wavelengths of the first excitation and excitations with the largest oscillator strengths, the main contributions to the first excited state, and the dipole moment (D), μ

Model	HOMO (eV)	LUMO (eV)	HL (eV)	OG (eV)	λ_{max} (nm)	f	Main contributions	μ (D)
					a **Values when solvent effects are taken into account for chloroform.**			
PBE	−4.60	−3.52	1.08	1.57	938	1.572	H → L (92.2%), H − 1 → L + 1 (4.8%)	0.350
B3LYP	−5.24, −5.21[a]	−3.07, −3.11[a]	2.17, 2.10[a]	1.93, 1.81[a]	641, 492, 390, 337, 684, 509, 398, 331[a]	2.558, 2.995[a]	H → L (98.3%), H → L (97.2)[a]	1.215, 1.487[a]
M06	−5.49, −5.47[a]	−2.88, −2.92[a]	2.60, 2.56[a]	2.12, 2.00[a]	585, 454, 368, 318, 619, 468, 375, 302[a]	2.971, 3.356[a]	H → L (90.0%), H − 1 → L + 1 (5.8%), H → L (88.3%), H − 1 → L + 1 (7.9%)[a]	1.176, 1.498[a]

In Fig. 2, we have plotted the isosurfaces (isovalue = 0.02) of the HOMO and LUMO, as well as the next nearest frontier orbitals, of the **BDT(CDTRH)$_2$** structure. Both the HOMO and LUMO extend over the main, nearly planar, body of the structure. However, there is a varying level of delocalization; the HOMO is more localized near the central part of the structure, while the LUMO is more localized towards the outer (edge) parts. The HOMO − 1 and LUMO + 1 do not exhibit significant contributions from the central structure, *i.e.* the benzodithiophene (**BDT**) moieties, but are rather localized mainly towards the outer parts, *i.e.*, the cyclopentadithiophene (**CPDT**) and the thiazole (**TA**) groups. To quantify the contributions of the moieties to the frontier orbitals, we have calculated the total and partial density of states (PDOS). The PDOS for **BDT(CDTRH)$_2$** is shown in Fig. S7 of ESI.† We divided **BDT(CDTRH)$_2$** into the **BDT**, **CPDT**, **TA** and the aliphatic groups. The contributions of the **BDT**, **CPDT**, and **TA** groups to the HOMO are 39.0%, 45.3%, and 14.9%, respectively, with only an 8.3% combined contribution from all the aliphatic groups. The corresponding contributions to the LUMO are 12.3%, 41.1% and 44.4%, respectively, and 2.2% combined from all the aliphatic groups. This is in agreement with our earlier observations on the localization of HOMO on the inner structure and the LUMO mainly on the outer structure. Taking into account that the first excitation is dominated by a HOMO to LUMO transition, this indicates at least a moderate (due to overlaps) charge transfer from the corresponding inner to the outer parts of the structure. The first significant contributions (16.2%) from the aliphatic groups are noted at lower energies, around −8.0 eV, which corresponds to the HOMO − 15 level.

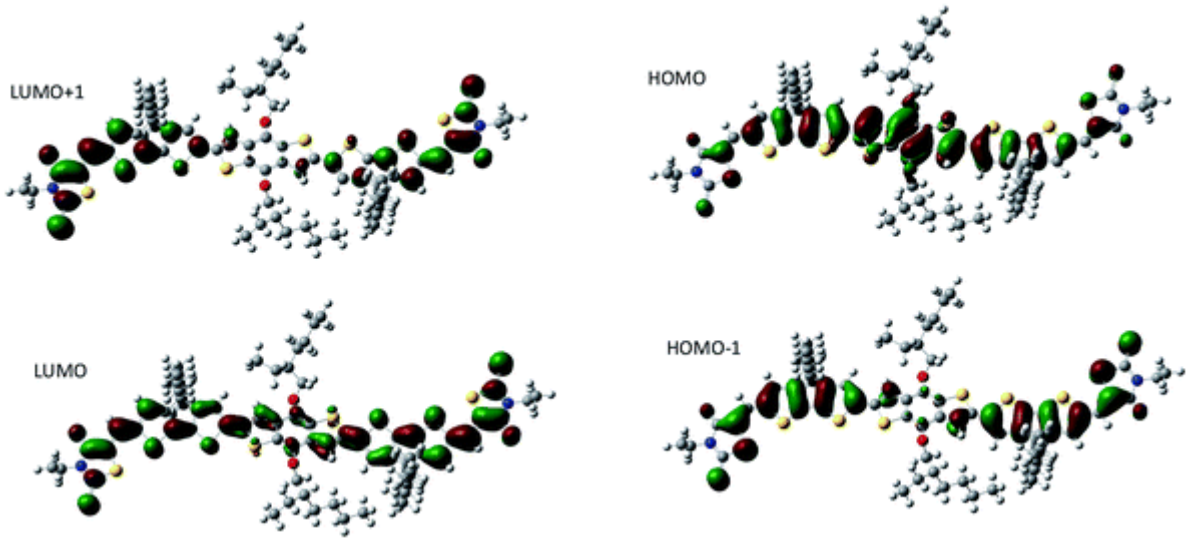

Fig. 2 Frontier and near frontier orbitals of **BDT(CDTRH)$_2$**.

In Fig. 3a, we show the UV/visible absorption spectra of the **BDT(CDTRH)$_2$** structure, calculated at the TD-DFT/M06 level of theory, both accounting for solvent effects for CF and in gas phase. The spectra have been produced by convoluting Gaussian functions with HWHM = 0.25 eV centered at the excitation wave numbers. In Fig. 3b, we also provide the corresponding spectra calculated using the B3LYP functional, which is in very good agreement with both the use of M06 and the experimental spectra. A characteristic absorption spectrum is found that displays a main band centered at 618 nm and three lower intensity bands at smaller wavelengths, specifically centered at 462 nm, 376 nm, and 307 nm. The calculated spectrum is in good agreement with the experimental one, with slightly overestimated wave numbers by about 5–35 nm, depending on the region (more overestimated at larger wavelengths). The wavelengths of the excitations with the largest oscillator strengths within these bands are given in Table 1.

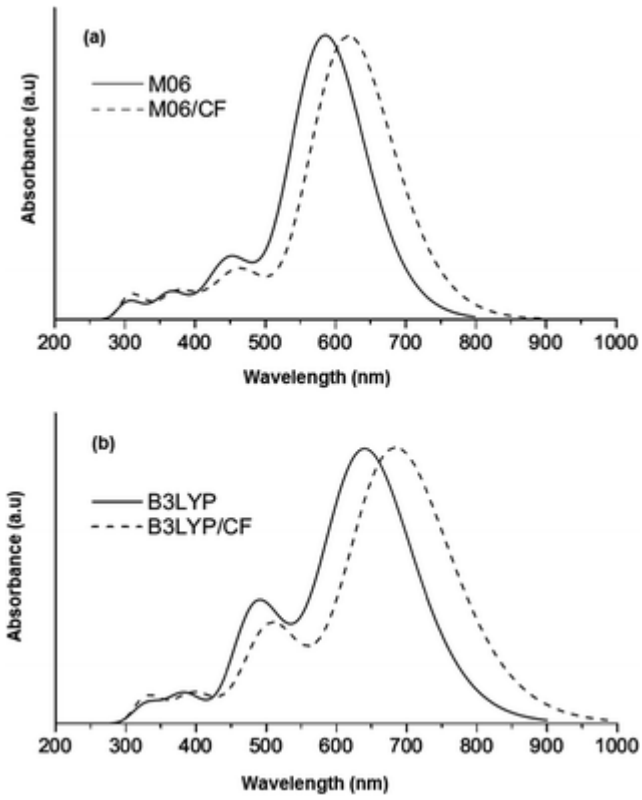

Fig. 3 Theoretical UV-vis absorption spectrum of **BDT(CDTRH)$_2$** (a) calculated using the M06 functional and (b) B3LYP functional.

Photovoltaic properties

In BHJ organic solar cells, the relative amounts of the donor and acceptor materials used in blend active layers is of great importance for their photovoltaic performance, because there should be a balance between the absorption and charge transporting network in the active layer. When the acceptor content is too low, the electron transporting ability will be limited, while when the acceptor content is too high, the absorbance and hole transport ability in the active layer will be decreased. BHJ devices were fabricated and optimized using different**BDT(CDTRH)$_2$**:$PC_{71}BM$ ratios, with device configuration being ITO/PEDOT:PSS/**BDT(CDTRH)$_2$**:$PC_{71}BM$/Al using conventional solution spin coating process. Various ratios of**BDT(CDTRH)$_2$**:$PC_{71}BM$ were investigated, and we found that the optimum weight ratio was 1 : 1. The normalized absorption spectra of **BDT(CDTRH)$_2$**:$PC_{71}BM$ blend thin film is shown Fig. 4. It can be seen from this figure that the absorption spectra of the blend is the combination of both **BDT(CDTRH)$_2$** and $PC_{71}BM$ absorption features, indicating that both components participate into the exciton generation and the photocurrent of the device.

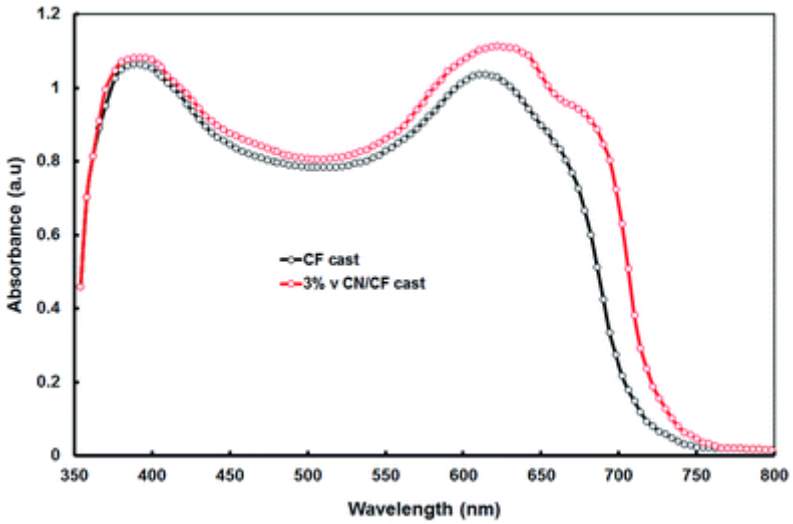

Fig. 4 Normalized absorption spectra of **BDT(CDTRH)$_2$** : $PC_{71}BM$ (1 : 1) films cast from CF and 3% v CN/CF solvents.

The current–voltage *J–V* characteristics, under sun-stimulated illumination (AM1.5, 100 mW cm^{-2}) of the BHJ organic solar cell with the **BDT(CDTRH)$_2$** : $PC_{71}BM$ blend of 1 : 1 weight ratio processed from chloroform (CF) is displayed in Fig. 5a, and the corresponding photovoltaic parameters are complied in Table 2. The device shows an overall PCE of 4.58% with J_{sc} = 8.66 mA cm^{-2}, V_{oc} = 0.98 V and FF = 0.54. The high value of V_{oc} is attributed to the deeper HOMO level of V_{oc}, because the maximum theoretical V_{oc} of the BHJ organic solar cells is directly related to the energy difference between the HOMO of the donor and the LUMO of the acceptor materials used in the active layer.

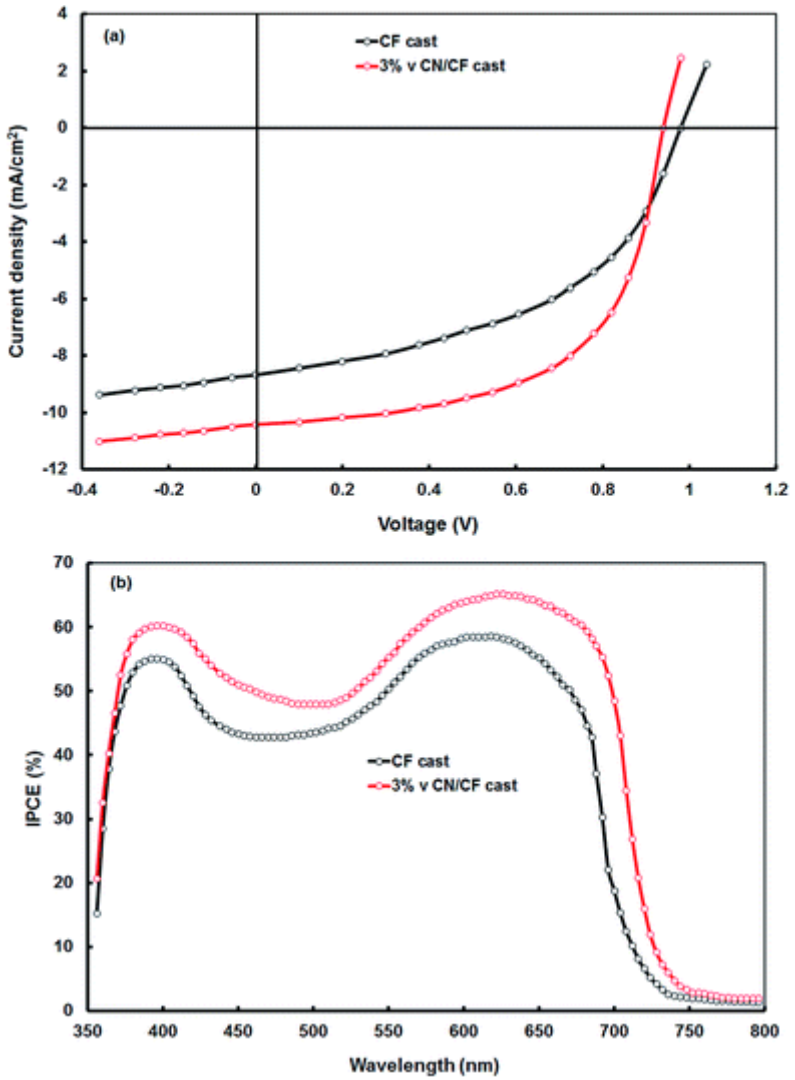

Fig. 5 (a) Current–voltage (*J*–*V*) characteristics under illumination and (b) IPCE spectra of solar cells based on **BDT(CDTRH)$_2$** : $PC_{71}BM$ (1 : 1) blend cast from CF and 3% v CN/CF solvents.

Table 2 Photovoltaic parameters of the **BDT(CDTRH)$_2$** : $PC_{71}BM$ (1 : 1) based solar cells

Solvent	J_{sc} **(mA cm^{-2})**	V_{oc} **(V)**	**FF**	**PCE (%)**
CF cast	8.66	0.98	0.54	4.58
CN/CF cast	10.42	0.94	0.62	6.07

To further improve the performance of these devices, we used CN as the solvent additive and varied the volume concentration in the blend solution from 1 to 4% and found that 3% v/v gave the best photovoltaic performance. The *J*–*V* characteristics of the best performing device are shown in Fig. 5a, and photovoltaic parameters are

summarized in Table 2. It achieved an overall PCE of 6.07% with J_{sc} of 10.42 mA cm^{-2}, V_{oc} = 0.94 V and FF = 0.62.

The improvement in the overall PCE of the device processed with CN/CF solvent was mainly due to a significant increase in the J_{sc}, as well as the FF. The J_{sc} is directly related to the light absorption ability of the active layer, as well as the better collection of charges at the electrodes, which is in direct relationship with the IPCE response, as well as with the film morphology. The **BDT(CDTRH)$_2$**:$PC_{71}BM$ film cast from CN/CF displays stronger absorption than the film cast from CF (Fig. 5). As shown in the absorption spectra of the blend cast from the CN/CF solvent, the absorption band of **BDT(CDTRH)$_2$** shifts slightly toward longer wavelengths and broadens. The absorption coefficient also increases. The vibronic shoulder peak is clearly observed at around 668 nm. The observed red shift in the absorption band of **BDT(CDTRH)$_2$** is attributed to the increase in order in the active layer film. The higher degree of crystallinity, as indicated by the red shift and vibronic shoulder in the absorption spectra of the blend, is also attributed to the enhanced π–π* conjugation. The increase in crystallinity of the active layer has been confirmed by XRD measurements, and it is discussed later. The enhanced value of FF may be ascribed to the high crystallinity and high carrier mobility of**BDT(CDTRH)$_2$** in the blend film.[38]

The IPCE spectra of the devices processed with CF and CN/CF are shown in Fig. 6b. The IPCE curves of the device covered a broad wavelength range: from 360 nm to 720 nm. The shape of the IPCE spectra of the devices closely resembles the optical absorption spectra of the active layers (Fig. 4). Moreover, the IPCE spectrum of **BDT(CDTRH)$_2$**:$PC_{71}BM$ solar cell processed with CN/CF was over 64% at 622 nm, whereas that of the device based on CF processed was about 56% (Fig. 5b). Additionally, the values of IPCE of the device processed with CF/CN at all absorption wavelengths were higher, leading to the enhanced value of J_{sc}.

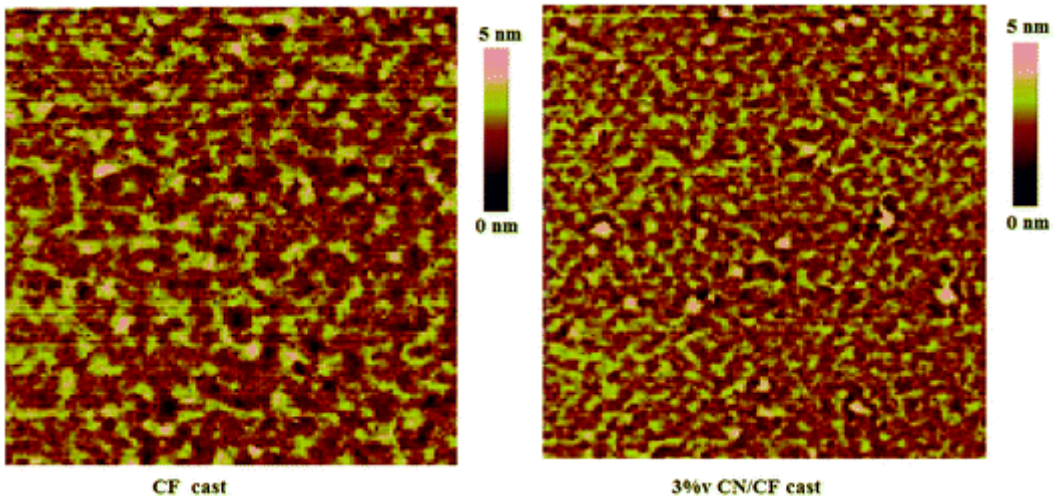

Fig. 6 AFM tapping mode height images (5 µm × 5 µm size)

of **BDT(CDTRH)$_2$**:$PC_{71}BM$ blend thin films cast from CF and 3% v CN/CF.

The surface morphology of the **BDT(CDTRH)$_2$**:$PC_{71}BM$ blend films processed from CF and CN/CF were investigated by atomic force microscopy (AFM). Fig. 6 shows the topographic images of the **BDT(CDTRH)$_2$**:$PC_{71}BM$ active layers processed with CF and CN/CF solvents. The film cast from CF shows apparent homogeneously mixed domains of **BDT(CDTRH)$_2$**and $PC_{71}BM$, with a surface root mean square (RMS) roughness of 2.45 nm. The incorporation of 3% v/v CN in the blend solution results in a significant change in the surface morphology of the film, with the RMS roughness of the film decreasing to 1.24 nm. Although the AFM images show that the morphology of the active layer has improved with the incorporation of CN, it is difficult to conclude that these features originate from the crystallization of the donor phase. Therefore, we have further investigated the domain sizes of the active layer films processed with CF and CN/CF solvents using TEM. In the TEM images (Fig. 7), well interpenetrating structures are formed with domain sizes of 30–40 nm and 15–20 nm for the active layers processed with CF and CN/CF solvents, respectively.

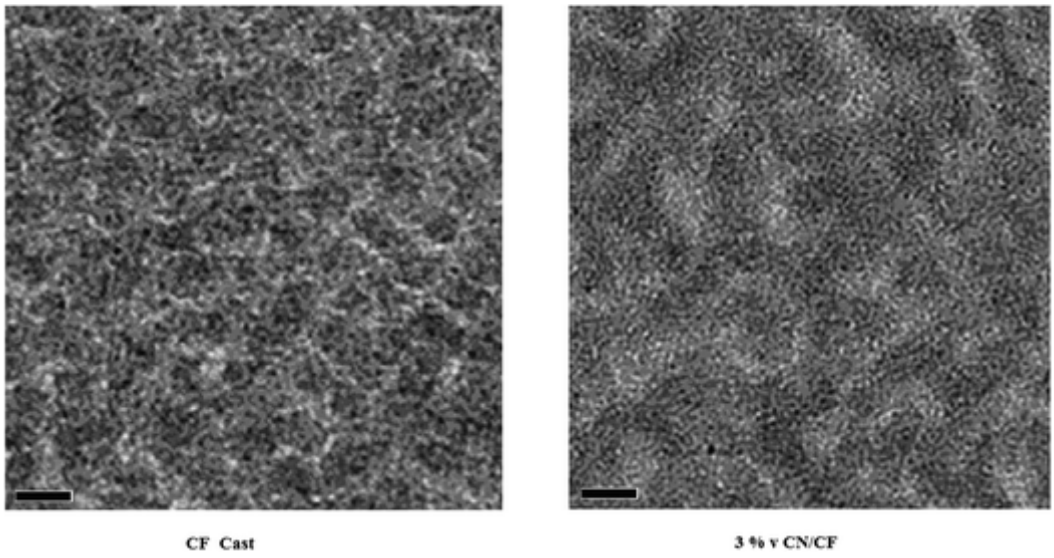

Fig. 7 TEM images of **VC90**:$PC_{71}BM$ blend thin films cast from CF and 3% v CN/CF, scale bar is 200 nm.

Fig. 8 shows the XRD pattern of the pristine **BDT(CDTRH)$_2$** and **BDT(CDTRH)$_2$**:$PC_{71}BM$ thin films cast from CF and CN/CF solvents. In the case of pristine **BDT(CDTRH)$_2$** cast from both CF and CN/CF solvents, a band centered at $2\theta = 5.64°$ was observed in the XRD pattern. However, the intensity of the band is more pronounced for the film cast from CN/CF, indicating an increase in crystallinity. It can be seen from the figure that when the **BDT(CDTRH)$_2$**:$PC_{71}BM$ blend is cast from CF, the diffraction peak becomes wider and the intensity is decreased. However, when the blend is cast from CN/CF solvent, the

intensity of the diffraction peak observed at $2\theta = 5.64°$ increases. Because the boiling point of CN is higher than that of CF, the film cast from the CN/CF solvent evaporates slowly and results in an increase in crystallinity. This change in crystallinity of the films agrees with the observed change in the absorption spectra. The increase in crystallinity of the blend helps to increase the holes' mobility in the blend.

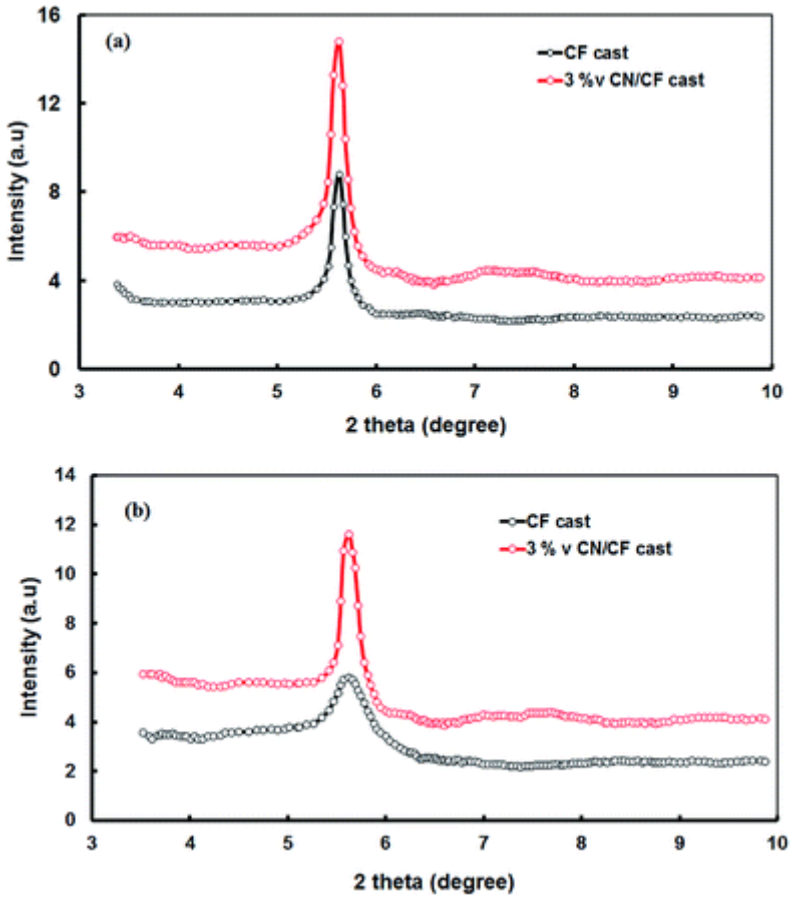

Fig. 8 XRD patterns of (a) pristine **BDT(CDTRH)$_2$** and (b) **BDT(CDTRH)$_2$**:$PC_{71}BM$ blend thin films cast from CF and 3% v CN/CF.

The charge carrier mobility in the BHJ active layer is critical for the BHJ organic solar cell. This is mainly due to the fact that after the exciton dissociation at the D/A interface, the amount of photogenerated charge carriers extracted at the electrode depends on the ratio of the charge carriers swept and those lost by recombination during their transport to the electrodes.[3e,39] In order to calculate the hole and electron mobility in the **BDT(CDTRH)$_2$**:$PC_{71}BM$ active layer, we measured the dark current of hole only and electron only devices, respectively, and then analyzed the results using the space charge limited current (SCLC) model:[40]

$$J = \frac{9}{8}\varepsilon_r\varepsilon_o\mu_h\frac{\left(V_{appl}-V_{bi}\right)^2}{L^3}$$

where ε_r, ε_o is the dielectric permittivity of the active layer and permittivity of free space, respectively, V_{appl} is applied voltage and V_{bi} is built in potential, μ_h is the hole mobility, L is the thickness of the active layer, and β is the field activation factor. Fig. 9 shows the experimental J–V characteristics of hole only devices with configuration ITO/PEDOT:PSS/**BDT(CDTRH)$_2$**:$PC_{71}BM$/Au. The hole mobilities were estimated from fitting the experimental results (solid lines in Fig. 9) and are about 2.3 × 10^{-5} cm^2 V^{-1} s^{-1} and 6.4 × 10^{-5} cm^2 V^{-1} s^{-1}, respectively for active layer processed with CN/CF and CF. The increase in the hole mobility with CN additive may be attributed to the increase in crystallinity and domain size. The electron mobilities were estimated from the J–V characteristics of the electron only devices ITO/Al/**BDT(CDTRH)$_2$**:$PC_{71}BM$/Al and are almost identical, *i.e.* 2.52 × $10^{-4}$$cm^2$ V^{-1} s^{-1} and 2.48 × 10^{-4} cm^2 V^{-1} s^{-1}, with and without CN additive, respectively. The difference between electron and hole mobilities is reduced in the **BDT(CDTRH)$_2$**:$PC_{71}BM$ film processed with CN/CF, leading to a more balanced charge transport.[41]

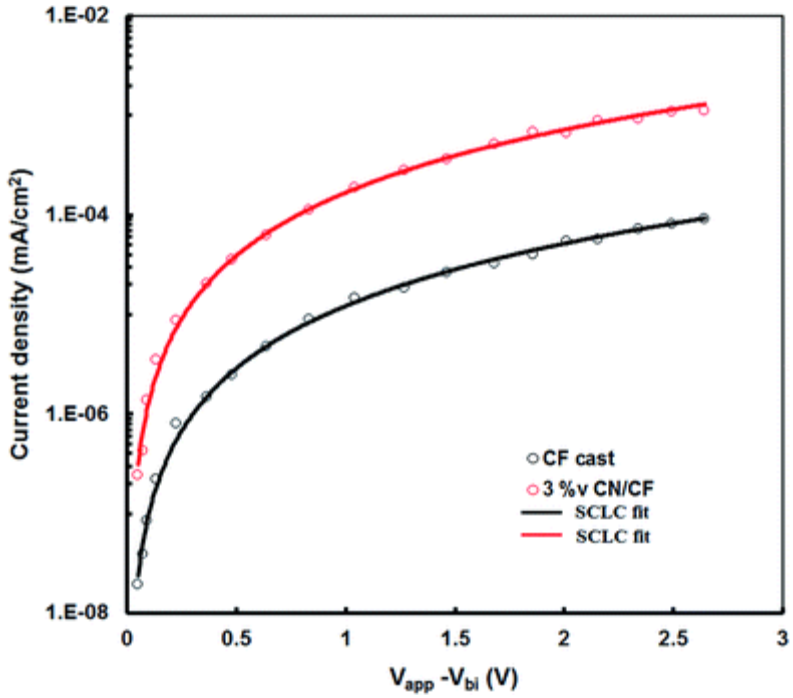

Fig. 9 Current–voltage (J–V) characteristics in dark for hole-only devices, using CF and 3% v CN/CF processed **BDT(CDTRH)$_2$**:$PC_{71}BM$ active layer blends.

Conclusion

In summary, we have synthesized an A–D–D′–D–A small molecule, **BDT(CDTRH)$_2$**, with a low bandgap (~1.72 eV) and investigated its optical and electrochemical properties (both theoretically and experimentally). The photophysical and electrochemical investigations of **BDT(CDTRH)$_2$** and $PC_{71}BM$ films proves that the **BDT(CDTRH)$_2$**:$PC_{71}BM$ blend can effectively harvest photons from visible to near infrared region of solar spectrum and transfer the electrons to $PC_{71}BM$ molecules, resulting in a photovoltaic effect. The solution processed BHJ solar cell based on **BDT(CDTRH)$_2$**:$PC_{71}BM$ processed from CF displayed a PCE of 4.58%. In order to

improve the PCE, the **BDT(CDTRH)$_2$**:$PC_{71}BM$ layer was spin cast from a mixture of 3% v/v CN/CF and the device showed a PCE of 6.07%, attributed to the enhancement in the J_{sc} and FF. This is the result of the enhanced IPCE response, the increase in the crystalline nature and the more favourable nanoscale morphology of the active layer with solvent additive and increase in hole mobility, which leads to a more balanced charge transport, and enhanced hole mobility in the BHJ active layer.

Acknowledgements

EP would like to thank MINECO for the project CTQ2013-47183 R and the support through Severo Ochoa Excellence Accreditation 2014-2018 (SEV-2013-0319). We would like to thank Prof. Athanassios G. Coutsolelos and Dr Georgios Charalambidis, University of Crete, Greece for the availability of the mass spectroscopy resources and support. We are also thankful to Material Science laboratory, MNIT, Jaipur and Department of Physics, LNMIT, Jaipur for the availability of device fabrication facilities and other characterization.

References

1 (a) A. Mishra and P. Bauerle, Angew. Chem., Int. Ed., 2012, 51,

2020; (b) Y. Lin, Y. Li and X. Zhan, Chem. Soc. Rev., 2012, 41,

4245; (c) V. Gupta, A. K. K. Kyaw, D. H. Wang, S. Chand,

G. C. Bazan and A. J. Heeger, Sci. Rep., 2013, 3, 1965; (d)

C. J. Takacs, Y. Sun, G. C. Welch, L. A. Perez, X. Liu,

W. Wen, G. C. Bazan and A. J. Heeger, J. Am. Chem. Soc.,

2012, 134, 16597; (e) J. Zhang, D. Deng, C. He, Y. He,

M. Zhang, Z.-G. Zhang, Z. Zhang and Y. Li, Chem. Mater.,

2011, 23, 817; (f) J. J. Jasieniak, B. B. Y. Hsu, C. J. Takacs,

G. C. Welch, G. C. Bazan, D. Moses and A. J. Heeger, ACS

Nano, 2012, 6, 8735; (g) J. Roncali, Acc. Chem. Res., 2009,

42, 1719; (h) Y. Lin, L. Ma, Y. Li, Y. Liu, D. Zhu and

X. Zhan, Adv. Energy Mater., 2014, 4, 1300626; (i) Y. Lin,

Z. G. Zhang, H. Bai, Y. Li and X. Zhan, Chem. Commun.,

2012, 48, 9655; (j) Y. Lin, Z. G. Zhang, Y. Li, D. Zhu and

X. Zhan, J. Mater. Chem. A, 2013, 1, 5128.

2 (a) J. Zhou, Y. Zuo, X. Wan, G. Long, Q. Zhang, W. Ni, Y. Liu,

Z. Li, G. He, C. Li, B. Kan, M. Li and Y. Chen, J. Am. Chem.

Soc., 2013, 135, 8484; (b) A. K. K. Kyaw, D. H. Wang,

D. Wynands, J. Zhang, T.-Q. Nguyen, G. C. Bazan and

A. J. Heeger, Nano Lett., 2013, 13, 3796; (c) B. Kan,

Q. Zhang, M. Li, X. Wan, W. Ni, G. Long, Y. Wang, X. Yang,

H. Feng and Y. Chen, J. Am. Chem. Soc., 2014, 136, 15529.

3 (a) J. Y. Zhou, Y. Zou, X. J. Wan, G. K. Long, Q. Zhang, W. Ni,

Y. S. Liu, Z. Li, G. R. He, C. X. Li, B. Kan, M. M. Li and

Y. S. Chen, J. Am. Chem. Soc., 2013, 135, 8484; (b) C. Q. Ma,

M. Fonrodona, M. C. Schikora, M. M. Wienk,

R. A. J. Janssenand and P. Bauerle, Adv. Funct. Mater., 2008,

18, 3323; (c) C. H. Cui, J. Min, C. L. Ho, T. Ameri, P. Yang,

J. Z. Zhao, C. J. Brabec and W. Y. Wong, Chem. Commun.,

2013, 49, 4409; (d) S. L. Shen, P. Jiang, C. He, J. Zhang,

P. Shen, Y. Zhang, Y. P. Yi, Z. J. Zhang, Z. B. Li and

Y. F. Li, Chem. Mater., 2013, 25, 2274; (e) Y. M. Sun,

G. C. Welch, W. L. Leong, C. J. Takacs, G. C. Bazan and

A. J. Heeger, Nat. Mater., 2012, 11, 44; (f) Y. S. Liu, Y. Yang,

C. C. Chen, Q. Chen, L. T. Dou, Z. R. Hong, G. Li and

Y. Yang, Adv. Mater., 2013, 25, 4657; (g) J. Y. Zhou,

X. J. Wan, Y. S. Liu, Y. Zou, Z. Li, G. R. He, G. K. Long,

W. Ni, C. X. Li, X. C. Su and Y. S. Chen, J. Am. Chem. Soc.,

2012, 134, 16345.

4 (a) J. Min, Y. N. Luponosov, T. Ameri, A. Elschner,

S. M. Peregudova, D. Baran, T. Heumuller, N. Li,

F. Machui, S. Ponomarenko and C. J. Brabec, Org. Electron.,

4900 2013, 14, 219; (b) J. Min, Y. N. Luponosov, A. Gerl,

M. S. Polinskaya, S. M. Peregudova, P. V. Dmitryakov,

A. V. Bakirov, M. A. Shcherbina, S. N. Chvalun,

S. Grigorian, N. K. Busies, S. A. Ponomarenko, T. Ameri

and C. J. Brabec, Adv. Energy Mater., 2014, 4, 1301234; (c)

J. Min, Y. N. Luponosov, D. Baran, S. N. Chvalun,

M. A. Shcherbina, A. V. Bakirov, P. V. Dmitryakov,

S. M. Peregudova, N. Kausch-Busies, S. A. Ponomarenko,

T. Ameri and C. J. Brabec, J. Mater. Chem. A, 2014, 2,

16135; (d) J. Min, Y. N. Luponosov, Z.-G. Zhang,

S. A. Ponomarenko, T. Ameri, Y. F. Li and C. J. Brabec, Adv.

Energy Mater., 2014, 4, 1400816; (e) H. X. Shang, H. J. Fan,

Y. Liu, W. P. Hu, Y. F. Li and X. W. Zhan, Adv. Mater.,

2011, 23, 1554; (f) W. W. Li, M. Kelchtermans,

M. M. Wienk and R. A. J. Janssen, J. Mater. Chem. A, 2013,

1, 15150.

5 (a) C.-Y. Kuo, W. Nie, H. Tsai, H.-J. Yen, A. D. Mohite,

G. Gupta, A. M. Dattelbaum, D. J. William, K. C. Cha,

Y. Yang, L. Wang and H.-L. Wang, Macromolecules, 2014,

47, 1008; (b) H. S. Chung, W.-H. Lee, C. E. Song, Y. Shin,

J. Kim, S. K. Lee, W. S. Shin, S.-J. Moon and I.-N. Kang,

Macromolecules, 2014, 47, 97.

6 J. A. Bartelt, J. D. Douglas, W. R. Mateker, A. El Labban,

C. J. Tassone, M. F. Toney, J. M. J. Fr´echet, P. M. Beaujuge

and M. D. McGehee, Adv. Energy Mater., 2014, 4, 1301733.

7 (a) J. Zhou, Y. Zuo, X. Wan, G. Long, Q. Zhang, W. Ni, Y. Liu,

Z. Li, G. He, C. Li, B. Kan, M. Li and Y. Chen, J. Am. Chem.

Soc., 2013, 135, 8484; (b) Y. Liu, C. Chen, Z. Hong, J. Gao,

Y. M. Yang, H. Zhou, L. Dou, G. Li and Y. Yang, Sci. Rep.,

2013, 3, 3356; (c) Y. Lin, L. Ma, Y. Li, Y. Liu, D. Zhu and

X. Zhan, Adv. Energy Mater., 2013, 3, 1166; (d) D. Patra,

T. Y. Huang, C. C. Chiang, R. O. V. Maturana, C. W. Pao,

K. C. Ho, K. H. Wei and C. W. Chu, ACS Appl. Mater.

Interfaces, 2013, 5, 9494.

8 (a) Y. Chen, X. Wan and G. Long, Acc. Chem. Res., 2013, 46, 2645; (b) J. Zhou, Y. Zuo, X. Wan, G. Long, Q. Zhang, W. Ni, Y. Liu, Z. Li, G. He, C. Li, B. Kan, M. Li and Y. Chen, J. Am. Chem. Soc., 2013, 135, 8484.

9 (a) Y. Sun, G. C. Welch, W. L. Leong, C. J. Takacs, G. C. Bazan and A. J. Heeger, Nat. Mater., 2012, 11, 44; (b) C. J. Takacs, Y. Sun, G. C. Welch, L. A. Perez, X. Liu, W. Wen, G. C. Bazan and A. J. Heeger, J. Am. Chem. Soc., 2012, 134, 16597; (c) X. Liu, Y. Sun, L. A. Perez, W. Wen, M. F. Toney, A. J. Heeger and G. C. Bazan, J. Am. Chem. Soc., 2012, 134, 20609.

10 (a) T. S. van der Poll, J. A. Love, T.-Q. Nguyen and G. C. Bazan, Adv. Mater., 2012, 24, 3646; (b) V. Gupta, A. K. K. Kyaw, D. H. Wang, S. Chand, G. C. Bazan and A. J. Heeger, Sci. Rep., 2013, 3, 1965.

11 J. Y. Zhou, Y. Zou, X. J. Wan, G. K. Long, Q. Zhang, W. Ni, Y. S. Liu, Z. Li, G. R. He, C. X. Li, B. Kan, M. M. Li and Y. S. Chen, J. Am. Chem. Soc., 2013, 135, 8484.

12 S. L. Shen, P. Jiang, C. He, J. Zhang, P. Shen, Y. Zhang, Y. P. Yi, Z. J. Zhang, Z. B. Li and Y. F. Li, Chem. Mater., 2013, 25, 2274.

13 Y. Liu, X. Wan, B. Yin, J. Zhou, G. Long, S. Yin and Y. Chen, J.

Mater. Chem., 2010, 20, 2464.

14 K. Schulze, C. Uhrich, R. Schuppel, K. Leo, M. Pieffer, E. Brier, E. Reinold and P. Bauerle, Adv. Mater., 2006, 18, 2872.

15 Y. Liu, X. Wan, F. Wang, J. Zhou, G. Long, J. Tian and Y. Chen, Adv. Mater., 2011, 23, 5387.

16 Y. Liu, X. Wan, F. Wang, J. Zhou, G. Long, J. Tian, J. You, Y. Yang and Y. Chen, Adv. Energy Mater., 2011, 1, 771.

17 J. Zhou, X. Wan, Y. Liu, G. Long, F. Wang, Z. Li, Y. Zuo, C. Li and Y. Chen, Chem. Mater., 2011, 23, 4666.

18 Y. Liu, Y. M. Yang, C. C. Chen, Q. Chen, L. Dou, Z. Hong, G. Li and Y. Yang, Adv. Mater., 2013, 25, 4657.

19 Z. Li, G. He, Y. Liu, J. Zhou, G. Long, Y. Zuo, M. Zhang and Y. Chen, Adv. Energy Mater., 2012, 2, 74.

20 J. Zhou, X. Wan, Y. Liu, Y. Zuo, Z. Li, G.He, G. Long,W. Ni, C. Li, X. Su and Y. Chen, J. Am. Chem. Soc., 2012, 134, 16345.

21 J. Zhou, Y. Zuo, X. Wan, G. Long, Q. Zhang, W. Ni, Y. Liu, Z. Li, G. He, C. Li, B. Kan, M. Li and Y. Chen, J. Am. Chem. Soc., 2013, 135, 8484.

22 Y. S. Liu, C.-C. Chen, Z. R. Hong, J. Gao, Y. M. Yang, H. P. Zhou, L. T. Dou, G. Li and Y. Yang, Sci. Rep., 2013, 3,

3356.

23 S. W. Chang, H. Waters, J. Kettle and M. Horie, Org. Electron.,

2012, 13, 2967.

24 R. Li, J. Liu, N. Cai, M. Zhang and P. Wang, J. Phys. Chem. B,

2010, 114, 4461.

25 Y. Y. Liang, D. Q. Feng, Y. Wu, S. T. Tsai, G. Li, C. Ray and

L. P. Yu, J. Am. Chem. Soc., 2009, 131, 7792.

26 (a) Y. Matsuo, Y. Sato, T. Niinomi, I. Soga, H. Tanaka and

E. Nakamura, J. Am. Chem. Soc., 2009, 131, 16048; (b)

M. C. Yuan, M. Y. Chiu, S. P. Liu, C. M. Chen and

K. H. Wei, Macromolecules, 2010, 43, 6936.

27 Z. Li, G. He, X. Wan, Y. Liu, J. Zhou, G. Long, Y. Zuo,

M. Zhang and Y. Chen, Adv. Energy Mater., 2011, 2, 74.

28 (a) M. C. Scharber, D. M¨uhlbacher, M. Koppe, P. Denk,

C. Waldauf, A. J. Heeger and C. J. Brabec, Adv. Mater.,

2006, 18, 789; (b) Y. Chen, Z. Du, W. Chen, Q. Liu, L. Sun,

M. Sun and R. Yang, Org. Electron., 2014, 15, 405.

29 J. P. Perdew, K. Burke and M. Ernzerhof, Phys. Rev. Lett.,

1996, 77, 3865.

30 A. Sch¨afer, C. Huber and R. Ahlrichs, J. Chem. Phys., 1994,

100, 5829.

31 K. Eichkorn, O. Treutler, H. ¨Ohm, M. H¨aser and R. Ahlrichs,

Chem. Phys. Lett., 1995, 240, 283.

32 (a) A. D. Becke, J. Chem. Phys., 1993, 98, 5648; (b) C. Lee,

W. Yang and R. G. Parr, Phys. Rev. B: Condens. Matter

Mater. Phys., 1988, 37, 785.

33 Y. Zhaoand and D. G. Truhlar, Theor. Chem. Acc., 2008, 120,

215.

34 M. J. Frisch, G. W. Trucks, H. B. Schlegel, G. E. Scuseria,

M. A. Robb, J. R. Cheeseman, G. Scalmani, V. Barone,

B. Mennucci, G. A. Petersson, H. Nakatsuji, M. Caricato,

X. Li, H. P. Hratchian, A. F. Izmaylov, J. Bloino, G. Zheng,

J. L. Sonnenberg, M. Hada, M. Ehara, K. Toyota,

R. Fukuda, J. Hasegawa, M. Ishida, T. Nakajima, Y. Honda,

O. Kitao, H. Nakai, T. Vreven, J. A. Montgomery, Jr,

J. E. Peralta, F. Ogliaro, M. Bearpark, J. J. Heyd,

E. Brothers, K. N. Kudin, V. N. Staroverov, R. Kobayashi,

J. Normand, K. Raghavachari, A. Rendell, J. C. Burant,

S. S. Iyengar, J. Tomasi, M. Cossi, N. Rega, J. M. Millam,

M. Klene, J. E. Knox, J. B. Cross, V. Bakken, C. Adamo,

J. Jaramillo, R. Gomperts, R. E. Stratmann, O. Yazyev,

A. J. Austin, R. Cammi, C. Pomelli, J. W. Ochterski,

R. L. Martin, K. Morokuma, V. G. Zakrzewski, G. A. Voth,

P. Salvador, J. J. Dannenberg, S. Dapprich, A. D. Daniels,

¨O. Farkas, J. B. Foresman, J. V. Ortiz, J. Cioslowski and

D. J. Fox, Gaussian 03, revision C.01, Gaussian, Inc.,

Wallingford CT, 2004.

35 TURBOMOLE (version 5.6), Universitat Karlsruhe, 2000.

36 D. Jacquemin, E. A. Perp`ete, I. Cio□ni, Adamo, R. Valero,

Y. Zhao and D. G. Truhlar, J. Chem. Theory Comput., 2010,

6, 2071.

37 S. Mathew, A. Yella, P. Gao, R. Humphry-Baker,

F. E. Curchod, N. Ashari-Astani, I. Tavernelli,

U. Rothlisberger, M. K. Nazeeruddin and M. Gr¨atzel, Nat.

Chem., 2014, 6, 242.

38 W. Guo, S. Wang, K. Sun, M. E. Thompson and S. R. Forrest,

Adv. Energy Mater., 2011, 1, 184.

39 (a) G. G. Malliaras, J. R. Salem, P. J. Brock and C. Scott, Phys.

Rev. B: Condens. Matter Mater. Phys., 1998, 58, 13411; (b)

V. D. Mihailetchi, J. Wildeman and P. W. Blom, Phys. Rev.

Lett., 2005, 94, 126602.

40 S. R. Cowan, R. A. Street, S. Cho and A. J. Heeger, Phys. Rev. B:

Condens. Matter Mater. Phys., 2011, 83, 035205.

41 (a)W. Wen, L. Ying, B. B. Y. Hsu, Y. Zhang, T. Q. Nguyen and

G. C. Bazan, Chem. Commun., 2013, 49, 7192; (b) J. Min,

Y. N. Luponosov, A. Gerl, M. S. Polinskaya,

S. M. Peregudova, P. V. Dmitryakov, A. V. Bakirov,

M. A. Shcherbina, S. N. Chvalun, S. Grigorian, N. Kaush-

Busies, S. A. Ponomarenko, T. Ameri and C. J. Brabec, Adv.

Energy Mater., 2014, 4, 1301234.